

Dynamic stiffness of deep foundations with inclined piles *

L.A. Padrón, J.J. Aznárez, O.Maeso, A.Santana

Instituto Universitario de Sistemas Inteligentes y Aplicaciones Numéricas en Ingeniería

(SIANI) Universidad de Las Palmas de Gran Canaria

Edificio Central del Parque Científico y Tecnológico

Campus Universitario de Tafira, 35017, Las Palmas de Gran Canaria, Spain

{lpadron,jjaznarez,omaeso}@siani.es

30 June 2011

Abstract

The influence of inclined piles on the dynamic response of deep foundations and superstructures is still not well understood and needs further research. For this reason, impedance functions of deep foundations with inclined piles, obtained numerically from a boundary element – finite element coupling model, are provided in this paper. More precisely, vertical, horizontal, rocking and horizontal-rocking crossed dynamic stiffness and damping functions of single inclined piles and 2×2 and 3×3 pile groups with battered elements are presented in a set of plots. The soil is assumed to be a homogeneous viscoelastic isotropic half-space and the piles are modeled as elastic compressible Euler-Bernoulli beams. Results for different pile group configurations, pile-soil stiffness ratios and rake angles are presented.

1 Introduction

The use of inclined piles in seismically active regions became highly discouraged after a series of earthquakes, occurred during the last decade of the 20th century, in which severe damage was observed in deep foundations with battered piles. As a consequence of these events, several seismic codes (e.g. AFPS 90 [1], Eurocode 8 - Part 5 [2]) recommend avoiding the use of this kind of foundations. However, the identification of the ultimate causes of those failures (rather related to incorrect design than to the pile inclination itself), together with an improvement on raked pile driving techniques, have contributed to increase again the popularity of inclined piles, which provide, in general, an improved capacity to withstand lateral loads when compared to vertical piles.

Nevertheless, regarding the response of the superstructure and the foundation itself, whether the presence of inclined piles improves or worsens the performance of structures submitted to dynamic (particularly seismic) loads, remains an open question, and different studies have found both detrimental and beneficial aspects in the use of raked piles. Several numerical analyses [3, 4, 5, 6] conclude that vertical piles should be preferred to raked ones because, in presence of soil movements, inclined piles tend to develop significantly larger loads along the pile shaft and, especially, at the connection to the pile cap, when compared to vertical piles. On the contrary, field evidence has been recollected [7, 8, 9] suggesting important beneficial effects regarding the use of battered piles. Moreover, different numerical results [10, 11, 12] show an

*This is the peer reviewed version of the following article: L.A. Padrón, J.J. Aznárez, O.Maeso, A.Santana, Dynamic stiffness of deep foundations with inclined piles, *Earthquake Engineering and Structural Dynamics* 2010; 39:1343-1367., which has been published in final form at <http://onlinelibrary.wiley.com/doi/10.1002/eqe.1000/pdf>. This article may be used for non-commercial purposes in accordance with Wiley Terms and Conditions for Self-Archiving. Figs 24 and 25 showed an incorrect y-scale, and has been reviewed.

improvement of the seismic response of both superstructure and foundation when inclined piles are used.

Consequently, it is apparent that further research is needed to be able to answer the question posed in the previous paragraph. In this respect, work must be done in different aspects of the same problem. One of the gaps that needs to be fulfilled is related to the influence of inclined piles on the dynamic stiffness of deep foundations, being this the area of contribution of this paper.

Impedance functions of deep foundations comprising exclusively vertical piles have been the object of extensive research, and a number of authors have provided dynamic stiffness functions for different cases and configurations [13, 14, 15, 16, 17, 18, 19, 20, 21, 22, 23, 24, 25, 26, 27, 28]. These results provided an insight into the dynamic behavior of piles and pile groups with respect to many different parameters and, in parallel, allowed the use of substructuring methods to estimate the response of structures founded on deep foundations.

An equivalent knowledge must be produced for configurations that include inclined piles, in such a way that the dynamic response of deep foundations with battered piles is better understood and that the scientific and engineering communities have the impedance functions needed to carry out substructuring analyses available.

Numerical results dealing with the dynamic response of raked piles have been contributed by different authors [3, 4, 5, 6, 10, 11, 12, 29] but, up to the authors' knowledge, impedance functions of inclined piles have been presented only by Giannakou et al. [30] for the case of a single pile embedded in a homogeneous or non-homogeneous soil deposit and previously by Mamoon et al. [20] for a specific case corresponding to a 3×3 pile group.

For all these reasons, impedance functions of single raked piles, together with those of 2×2 and 3×3 groups with inclined piles, embedded in a viscoelastic half-space, are presented in this paper. These results have been obtained numerically making use of a boundary element – finite element formulation, in which the soil region is modeled by means of the three-dimensional boundary element method, the piles rigidity is introduced later into the system by using mono-dimensional finite elements, and the pile-soil interaction is modeled through the establishment of equilibrium and compatibility conditions between piles and soil. For this purpose, a set of internal points and internal load lines must be introduced in the boundary element model for the soil. With this approach, the emptying of the soil at the piles location does not need to be explicitly modeled with boundary elements, which provides a great reduction in terms of number of degrees of freedom, mesh complexity and meshing efforts in comparison with a pure multi-region boundary element approach. Besides, it has been shown that the present formulation is able to produce accurate results in spite of this simplifying assumption.

The first section outlines the numerical formulation used herein, which is an enhancement of a model previously developed and implemented exclusively for vertical piles [31, 32]. In the following two sections, the parameters needed to define the geometry are described, the problem at hand (i.e. the impedance problem) is defined, and a series of validation results are presented. Then, stiffness and damping functions corresponding to single raked piles and 2×2 and 3×3 groups with inclined elements are shown in a set of dimensionless plots. The importance and main trends observed in the influence of the rake angle in the dynamic response of the foundations are pointed out.

2 Numerical model

The boundary element method is used herein to model the dynamic response of the soil region taking into account the internal loads arising from the pile-soil interaction. These loads are modeled as distributions of tractions applied on a line defined by the pile axis, and are named 'load-lines'. On the other hand, the piles rigidity is introduced later into the system by using finite elements. The whole approach, together with the definition of the geometrical parameters of the problem, is depicted in figure 1.

Let the soil be considered as a linear, homogeneous, isotropic, viscoelastic, unbounded region Ω with boundary Γ . The boundary integral equation for a time-harmonic elastodynamic state defined in the domain Ω can be written in a condensed and general form as

$$\mathbf{c}^k \mathbf{u}^k + \int_{\Gamma} \mathbf{p}^* \mathbf{u} d\Gamma = \int_{\Gamma} \mathbf{u}^* \mathbf{p} d\Gamma + \sum_{j=1}^{n_p} \left[\int_{\Gamma_{p_j}} \mathbf{u}^* \mathbf{q}^{s_j} d\Gamma_{p_j} + \mathbf{r}_j^k \mathbf{f}_{s_j} \right] \quad (1)$$

where \mathbf{c}^k is the local free term matrix at collocation point ' k ', \mathbf{u} and \mathbf{p} represent the displacement and traction fields in the three directions of space, \mathbf{u}^* and \mathbf{p}^* are the elastodynamic fundamental solution tensors on the boundary Γ due to a time-harmonic concentrated load at point ' k ', n_p is the number of piles, and Γ_{p_j} represents the pile-soil interface along the load-line j . In equation (1), the two terms between brackets represent the contribution of the internal loads, being \mathbf{q}^{s_j} and \mathbf{f}_{s_j} vectors containing the tractions (acting within the soil) along the pile-soil interface. More precisely, \mathbf{f}_{s_j} represents a point load placed at the tip of the pile, while \mathbf{q}^{s_j} is the distribution of interaction loads, along the pile shaft, applied on a line defined by the pile axis, both forces \mathbf{f}_{s_j} and \mathbf{q}^{s_j} coming from the pile-soil interaction along the different interfaces. On the other hand, \mathbf{r}_j^k represents the corresponding \mathbf{u}^* tensor computed at the tip of the pile. However, a singularity arises when the collocation point ' k ' coincides with the tip node of the pile. In such a case, this term can be computed by considering the force at the tip of the pile as a vector of uniformly distributed tractions over a circular surface with radius $R_p = \sqrt{A/\pi}$, which yields a regular integral [31, 32], being A the area of the pile section.

Following the usual procedure in the boundary element method, the numerical solution of equation (1) requires the discretization of the boundary surface. In this case, quadratic elements of six and nine nodes have been used. Then, over each boundary element, displacement and traction fields \mathbf{u} and \mathbf{p} are approximated in terms of their values at nodal points ($\bar{\mathbf{u}}$ and $\bar{\mathbf{p}}$) making use of a set of polynomial interpolation functions [33]. The evaluation of the first two integrals of equation (1), when the collocation point belongs to the integrated element, involves the solution of the singularities of order $O(1/r)$ and $O(1/r^2)$ present in the fundamental solution tensors \mathbf{u}^* and \mathbf{p}^* , respectively. The first kind of singularity, also known as *weak singularity*, is addressed through an element subdivision technique in conjunction with a co-ordinate transformation procedure to make the integrand regular. The second type of terms, called *strongly-singular terms*, are evaluated by identifying the $O(1/r^2)$ terms and splitting them up into a regular surface integral and a linear integral over the element perimeter. Then, singularities get canceled with the contribution of adjacent elements. More details on the numerical details of the method can be found in [32]. Regarding the load lines and the evaluation of the last two terms of equation (1), the distribution of tractions \mathbf{q}^{s_j} is approximated, according to the corresponding pile finite-element discretization into nodes and elements and to the proper interpolation functions [31, 32], in terms of its values $\bar{\mathbf{q}}^{s_j}$ defined at a series of internal nodes. Integrals over Γ_{p_j} are computed numerically as monodimensional integrals extended along a line defined by the pile axis. However, these integrals have a singularity at the collocation point when written for a node belonging to the integrated element. The arising singularity can be avoided through the use of a non-nodal collocation strategy, as depicted in figure 6, which is equivalent to integrating over a cylinder of radius R_p where tractions $\mathbf{f}_{s_j}/(2\pi R_p)$ are applied. As for the non-nodal collocation strategy, the integral is computed for four collocation points symmetrically placed around the pile, so that the term can be computed as the pondered sum of the four.

Now, equation (1) can be written for all boundary nodes in Γ and all internal nodes in Γ_{p_i} , yielding, respectively, the following two matrix equations

$$\mathbf{H}^{ss} \bar{\mathbf{u}} - \mathbf{G}^{ss} \bar{\mathbf{p}} - \sum_{j=1}^{n_p} \mathbf{G}^{sp_j} \bar{\mathbf{q}}^{s_j} - \sum_{j=1}^{n_p} \mathbf{r}_j^s \mathbf{f}_{s_j} = 0 \quad (2)$$

$$\bar{\mathbf{u}}^{p_i} + \mathbf{H}^{p_i s} \bar{\mathbf{u}} - \mathbf{G}^{p_i s} \bar{\mathbf{p}} - \sum_{j=1}^{n_p} \mathbf{G}^{p_i p_j} \bar{\mathbf{q}}^{s_j} - \sum_{j=1}^{n_p} \mathbf{r}_j^{p_i} \mathbf{f}_{s_j} = 0 \quad (3)$$

where \mathbf{H} and \mathbf{G} are coefficient matrices obtained by integration over the elements of the fundamental solution times the corresponding shape functions, $\bar{\mathbf{u}}$ and $\bar{\mathbf{p}}$ are the vectors of nodal displacements and tractions of the boundary elements, and $\bar{\mathbf{u}}^{p_i}$ is the vector of nodal displacements along load-line i .

On the other hand, piles are discretized using three-node beam elements with 13 degrees of freedom: three displacements on each node and two rotations at each of the ends. Linear axial deformation is allowed and pile flexural behavior is modeled according to the Euler-Bernoulli beam theory, but torsional response is not included in the model. After the discretization process, the dynamic behavior of pile j can be represented, in the finite-element sense, by a matrix equation

$$(\mathbf{K}_j - \omega^2 \mathbf{M}_j) \bar{\mathbf{u}}^{p_j} = \mathbf{f}_j^{ext} - \mathbf{Q}_j \bar{\mathbf{q}}^{s_j}, \quad (4)$$

where ω is the circular frequency of excitation, $\bar{\mathbf{u}}^{p_j}$ is the vector of nodal translation and rotation amplitudes along the pile, \mathbf{f}_j^{ext} includes the external forces acting at the top and the tip of the pile, \mathbf{K}_j and \mathbf{M}_j are the stiffness and mass matrices of the pile, and \mathbf{Q}_j is the matrix that transforms these nodal traction components to equivalent nodal forces. As usual, matrices \mathbf{K}_j , \mathbf{M}_j and \mathbf{Q}_j are expressed herein as global matrices, obtained following the general assembly process of the finite element method from the elemental matrices defined for a general vertical element [31, 32] and after pre and post multiplying by the corresponding rotation matrices in order to adapt to the pile inclination.

Now, imposing equilibrium and compatibility conditions along the load lines, and prescribing boundary conditions, equations (2), (3) and (4) can be rearranged in a system of equations of the type

$$\mathbf{A} \{ \bar{\mathbf{u}}, \bar{\mathbf{p}}, \bar{\mathbf{q}}^s, \bar{\mathbf{u}}^p, \mathbf{f}_s \}^T = \mathbf{B} \quad (5)$$

which represents the soil-pile system, and where \mathbf{A} and \mathbf{B} are the square matrix of coefficients and the known r.h.s. vector, respectively.

3 Geometrical parameters and dynamic stiffness problem definitions

As said before, the main objective of this paper is obtaining all the relevant impedance functions corresponding to a deep foundation with inclined piles in a homogeneous half-space. In this section, the impedance problem is defined together with all the geometrical parameters and material properties that are considered in this work.

The main geometrical parameters of the system are depicted in figure 1. Piles will be arranged in square regular groups, being all piles identical in length (L), diameter (d) and material properties. s is used to denote the distance between centers of adjacent pile heads, while θ refers to the angle between the pile axis and the vertical. Pile heads are assumed to be constrained (through fixed-head connection conditions) to a rigid mass-less pile cap which is not in contact with the ground surface. Pile groups configurations are always symmetrical with respect to planes xz and yz .

All results presented in the following sections correspond to problems sharing the following properties: soil internal hysteretic damping coefficient $\beta_s = 0.05$, soil-pile densities ratio $\rho_s/\rho_p = 0.7$, piles aspect ratio $L/d = 15$, soil Poisson's ratio $\nu_s = 0.4$, and pile-soil modulus ratios $E_p/E_s = 10^3$ (soft soil) and $E_p/E_s = 10^2$ (stiff soil).

In order to compute the foundation impedance functions, pile heads are subjected to forced vibration in each of the oscillation modes (vertical, horizontal and rocking). Then, the ratio between each component of the vector of forces (and moments) applied at the pile top and the corresponding term of the resulting vector of displacements (and rotations) at the same point, yields the dynamic stiffness matrix K_{ij} of the foundation. For pile groups, the impedances are obtained from the proper combination of the contributions of each pile. Vertical, horizontal, rocking and horizontal-rocking coupling terms of the impedance matrix will be denoted by

K_{zz} , K_{hh} , K_{rr} and K_{rh} respectively. For a time-harmonic excitation, these impedance functions depend on the frequency of excitation ω , and they are usually written as $K_{ij} = k_{ij} + ia_o c_{ij}$, where k_{ij} and c_{ij} are the frequency dependent dynamic stiffness and damping coefficients, respectively, $a_o = \omega d/c_s$ is the dimensionless frequency and c_s is the soil shear-wave velocity. For pile groups, when the foundation configuration is such that vibration modes along x and y horizontal axes yield different swaying and rocking impedances, both modes are computed and plotted.

4 Comparison results

The formulation presented above was implemented in a previously existent multi-region BEM FORTRAN code [28, 34]. The aim of this section is the validation of this formulation (and its implementation) through a set of comparison results corresponding, firstly, to values for the static stiffness of a single battered pile, and secondly, to dynamic stiffness and damping functions for 2×2 pile groups.

4.1 Static stiffness of a single battered pile

Using a 3-D finite-element model, and taking Gazetas' analytical expressions for the static stiffnesses of vertical piles [35] as a starting point, Giannakou et al. [30] produced the following equation as an estimation of the horizontal stiffness of a single battered pile embedded in a homogeneous elastic half-space, as a function of the rake angle θ :

$$k_{hh} \simeq 1.08 E_s d (1 + 4 \tan^2 \theta) \left(\frac{E_p}{E_s} \right)^{0.21(1+4 \tan^2 \theta)^{-1}} \quad (6)$$

According to Giannakou et al. [30], rocking and horizontal-rocking cross static stiffnesses, on the contrary, are independent of θ , and can be computed using the expressions provided by Gazetas [35] for vertical piles as:

$$k_{rr} \simeq 0.15 E_s d^3 \left(\frac{E_p}{E_s} \right)^{0.75} ; \quad k_{hr} \simeq -0.22 E_s d^2 \left(\frac{E_p}{E_s} \right)^{0.50} \quad (7)$$

On the other hand, and based on results indicating that axial and lateral displacements of a pile subjected to axial and lateral loads are almost independent of the pile inclination, Poulos & Davis [15] provide a simplified methodology to estimate, among other parameters, the vertical and horizontal displacements of a battered pile subjected to vertical and horizontal loads, from which horizontal stiffness can be computed.

In figure 3, static stiffnesses of a single battered pile embedded in a homogeneous elastic half-space obtained with the BEM-FEM coupling formulation are compared with equations (6) and (7) by Giannakou et al., and with results from Poulos & Davis [15] for the same problem. Regarding the horizontal stiffness, it can be seen that the results obtained using the formulation presented here are always above those of Poulos & Davis (differences ranging 18% to 8% for the values of θ and E_p/E_s analyzed herein) though both curves are parallel for each inclination angle. On the contrary, the difference with the expression provided by Giannakou et al. (which produces the highest estimations) increases with the rake angle. This disagreement, ranging 0% to 30%, may be caused by an extra stiffness provided by the fact that the soil is bounded in finite-element model used by Giannakou et al. Nonetheless, the estimations of the rocking and horizontal-rocking crossed stiffnesses are in very good agreement, coinciding in the hypothesis that the rocking stiffness is completely independent of the rake angle, while the BEM-FEM model predicts a slight decrease in the magnitude of the crossed stiffness for increasing inclination angle θ .

4.2 Impedance functions of 2×2 pile groups

Some advanced 3-D multi-region boundary element codes for time-harmonic elastodynamic problems have been used to analyze the dynamic behavior of piles (see e.g. [26, 27, 28, 34]). In this section, the computation of the impedance functions of pile groups by the method proposed here is going to be validated against results obtained using the code presented in [28].

3-D boundary element formulation.

In this multi-region boundary element formulation, both soil and piles are modeled as continuum isotropic homogeneous linear viscoelastic regions with their actual geometries. The boundary integral representation of the displacements in each domain (soil and each pile) corresponds to expression (1) but leaving the right hand side only with the first term. For the specific case of a single floating pile embedded in a viscoelastic half-space, the boundary element equations for each region (pile and soil) in partitioned form are:

$$\mathbf{H}_1^p \mathbf{u}_1^p + \mathbf{H}_2^p \mathbf{u}_2^p = \mathbf{G}_1^p \mathbf{p}_1^p + \mathbf{G}_2^p \mathbf{p}_2^p \quad (8)$$

$$\begin{bmatrix} \mathbf{H}_2^{pp} & \mathbf{H}_2^{ps} \\ \mathbf{H}_3^{sp} & \mathbf{H}_3^{ss} \end{bmatrix} \begin{bmatrix} \mathbf{u}_2 \\ \mathbf{u}_3 \end{bmatrix} = \begin{bmatrix} \mathbf{G}_2^{pp} & \mathbf{G}_2^{ps} \\ \mathbf{G}_3^{sp} & \mathbf{G}_3^{ss} \end{bmatrix} \begin{bmatrix} \mathbf{p}_2 \\ \mathbf{p}_3 \end{bmatrix} \quad (9)$$

corresponding equations (8) and (9) to pile and soil regions, respectively. According to figure 4, sub-indexes 1 to 3 of the above equations correspond, respectively, to the pile connection with the rigid cap where nodal displacements are known (Γ_1), to the pile-soil interface (Γ_2), and to the soil free-traction ground surface (Γ_3). Imposing, on the above expressions, external boundary conditions together with compatibility and equilibrium along the pile-soil interfaces, the combined equations for the coupled impedance problem can be written as

$$\begin{bmatrix} -\mathbf{G}_1^p & \mathbf{H}_2^p & \mathbf{G}_2^p & \mathbf{0} \\ \mathbf{0} & \mathbf{H}_2^{pp} & -\mathbf{G}_2^{pp} & \mathbf{H}_2^{ps} \\ \mathbf{0} & \mathbf{H}_3^{sp} & -\mathbf{G}_3^{sp} & \mathbf{H}_3^{ss} \end{bmatrix} \begin{bmatrix} \mathbf{p}_1^p \\ \mathbf{u}_2 \\ \mathbf{p}_2 \\ \mathbf{u}_3 \end{bmatrix} = \begin{bmatrix} -\mathbf{H}_1^p \hat{\mathbf{u}} \\ \mathbf{0} \\ \mathbf{0} \\ \mathbf{0} \end{bmatrix} \quad (10)$$

All boundaries (pile-soil interfaces, pile-cap interfaces and ground surface) are discretized into a finite number of quadratic nine-node and six-node boundary elements. Details of one of the used meshes in this work are shown in figure 4. Note that, due to the problem symmetries, only one quarter of the geometry needs to be discretized.

This multi-region BEM code, being more rigorous and versatile than the simplified BEM-FEM coupling scheme presented before, presents clear disadvantages when it comes to performing parametric studies. Such disadvantages are all related to the relatively high number of degrees of freedom involved in a boundary element model and also to the amount of work needed to produce the mesh corresponding to each one of the configurations to analyze. Both negative aspects are clearly improved by the coupling formulation, where the number of degrees of freedom is radically reduced, and the pile discretization, much more simple to define, is independent of the soil mesh.

Validation results

In this section, comparison results are shown for several configurations of 2×2 inclined pile groups. Three different rake angles have been considered for these plots: $\theta = 10^\circ$, 20° and 30° . The first case corresponds always to a pile separation ratio of $s/d = 5$, while the other two correspond to $s/d = 10$. Also, for $\theta = 10^\circ$ and 30° , piles are always inclined parallel or perpendicular to the direction of excitation. On the other hand, the configuration used for $\theta = 20^\circ$ corresponds to a case in which the piles are inclined, symmetrically, along the cap diagonals (see table 1). Results are shown for the two different pile-soil stiffness ratios considered in this paper.

Figures 5 to 8 present horizontal, vertical, rocking and horizontal-rocking crossed dynamic stiffness and damping functions for the configurations described above. Results corresponding to the boundary element – finite element coupling formulation presented in section 2 are labeled as “BEM-FEM” and plotted using points, while those obtained from the multi-region boundary element code are labeled as “BEM-BEM” and plotted using solid lines. In the horizontal and rocking cases, results are provided for excitation modes along both horizontal axes. It can be seen that a very good agreement exists between the BEM-FEM coupling scheme used in the following section and the more rigorous boundary element code.

5 Impedances of deep foundations with inclined piles

This section provides dynamic stiffness and damping functions of single inclined piles, and 2×2 and 3×3 pile groups with battered elements, according to the geometrical parameters and material properties defined in section 3. Results corresponding to rake angles $\theta = 0^\circ$ (vertical piles) 10° , 20° and 30° are presented, and also two different pile-soil stiffness ratios have been considered: $E_p/E_s = 1000$ (solid lines) and $E_p/E_s = 100$ (dashed lines).

All four impedance functions corresponding to a single inclined pile are presented in figure 9. In all cases, impedance functions are basically parallel for different rake angles. The horizontal stiffness of the battered pile increases with the rake angle (with a growing increment rate with θ), behavior that can be explained by the fact that the pile axial stiffness (much greater than the flexural stiffness) is mobilized when the pile is inclined. On the contrary, vertical impedances decrease with θ , which can be understood because now the vertical load is not only withstood by the pile axial stiffness but also by flexural deformation. Horizontal-rocking crossed impedances also decrease with θ , while rocking impedances are independent of the inclination angle, as seen in section 4.1 for the static values.

Next, figures 10 to 17 contain the horizontal, vertical, rocking and horizontal-rocking crossed stiffness and damping functions, alternatively for $s/d = 5$ and $s/d = 10$, of 2×2 pile groups. Similarly, figures 18 to 25 show the same information corresponding to 3×3 pile groups. Throughout these two sets of plots, in which the stiffness and damping functions are plotted in the upper and lower parts of the figures, respectively, the foundation configuration and the vibration mode corresponding to every pair of functions are specified using a sketch of the problem. The figures corresponding to the horizontal-rocking crossed impedances do not contain these sketches, but follow always the same pattern of the previous figures. A very important influence of pile inclination can be appreciated in virtually all impedance functions analyzed herein.

As expected, the horizontal stiffness and damping functions of the considered foundations experience a substantial increment when the piles are inclined in the direction of excitation (right plots). This increment exists for the static value and for all the frequency range, in such a way that the curves for different inclinations do not cross each other and, at the same time, the frequency corresponding to the peak value decreases slightly for increasing θ . These comments are valid for both 2×2 and 3×3 pile groups and for the s/d and E_p/E_s values considered in the study.

On the contrary, when piles are inclined perpendicularly to the direction of movement (left plots), the effect of pile inclination depends on the frequency range and pile separation, in such a way that, for $s/d = 5$ the stiffness increases with θ when $a_o \lesssim 0.6$ and decreases very significantly for higher frequencies, while for $s/d = 10$ the stiffness increases when $a_o \lesssim 0.2$, decreases when $0.2 \lesssim a_o \lesssim 0.6$ and increases for higher frequencies, being the variations less important than in the previous case. These can be considered to be general conclusions for both s/d values if the comments are made in reference to a frequency slightly below the global maxima, as the stiffness increases with θ below such a frequency and decreases for higher a_o . It can also be seen that the frequency of the peak value diminishes with the rake angle, as would correspond to higher pile separation ratios, while the static stiffness does not change significantly in this case.

Similarly to what happens with the stiffness functions, horizontal damping increases with θ

for all frequencies and for both s/d values when piles are inclined in the direction of movement, while it decreases throughout most of the frequency range when piles are inclined perpendicularly to the direction of movement, being the influence in this case smaller for $s/d = 10$.

Cases corresponding to the intermediate configuration (central plots) present a somehow intermediate behavior, with impedance functions increasing with the rake angle in all the frequency range for $s/d = 10$ (as in the results shown on the right) but with smaller peak values than those corresponding to the $\theta = 0^\circ$ for $s/d = 5$ (as in the results shown on the left).

As for the vertical impedances, the presence of inclined piles makes the sharp peaks associated to the pile-soil-pile interaction effect to fade away quite strongly. At the same time, the frequency at which those peaks take place decreases with the rake angle, for all the parameters and configurations analyzed. The direction of the variation in the vertical stiffness of the foundation due to pile inclination depends strongly on the frequency range of interest. For $s/d = 5$, the impedance increases for $a_o \lesssim 0.5$ and decreases for higher frequencies, while for $s/d = 10$ this limit frequency is $a_o \simeq 0.2$. Also, from an engineering point of view, it can be said that, regarding the vertical impedances, the two configurations analyzed for each pile group are equivalent for a certain rake angle. Note that all these conclusions presented in the last five paragraphs are applicable to both 2×2 and 3×3 pile groups.

On the other hand, it is important to highlight the fact that, while the rocking impedance of a single battered pile has been shown to be independent of the rake angle, the rocking impedance of a pile group is highly dependent on this parameter, which can be understood because, in this last case, rocking and vertical modes are coupled in each pile. Far from what happened for horizontal and vertical vibration modes, the way in which the rocking impedance functions are modified by the rake angle is completely different for 2×2 or 3×3 pile groups. For 3×3 pile groups, and regarding these impedance functions, the three configurations are equivalent from an engineering point of view, which is not the case for 2×2 pile groups. Again for 3×3 pile groups, the magnitude of the local maxima related to the pile group interaction effects decreases significantly for growing rake angles in all cases. On the contrary, for 2×2 pile groups, the presence of battered piles is less important, except when the axis of rotation is perpendicular to the plane in which the piles are inclined, case in which the peak values increase strongly in the presence of inclined piles. In general, the increment or decrease of stiffness with the rake angle is, mainly for $s/d = 10$, extraordinary dependent on a_o ,

Finally, it is apparent from figures 16, 17, 24 and 25 that the inclination of piles perpendicularly to the direction of a horizontal movement (left plots) has little influence on the horizontal-rocking crossed impedance functions, but a very important one on the other two types of configurations (central and right plots). Dynamic stiffness and damping functions can even change sign for different rake angles, which implies significant differences in the dynamic response of a superstructure.

6 Conclusions

The paper presents dynamic stiffness and damping functions of single battered piles, and of 2×2 and 3×3 pile groups with inclined elements, embedded in a homogeneous viscoelastic half-space. Numerical results, obtained from a boundary element – finite element code, are shown for different pile group configurations, rake angles and soil properties.

Regarding the dynamic response of single battered piles, the fact that the axial stiffness of a pile is much higher than its transversal stiffness (relative to the pile axis) makes it easy to understand that the horizontal impedance of an inclined pile increases with the rake angle due to the combination of axial and flexural stiffnesses to withstand horizontal loads. For the same reason, the pile vertical impedance decreases with the inclination angle because transversal stiffness starts to take part in the vertical mode. Also intuitive is the observation that the rocking impedance of a single pile is basically independent of the inclination angle.

It has also been shown that, in the case of a single pile, the influence of the rake angle

on the dynamic stiffness functions can be extrapolated from the static values. This is not the case for pile groups, where the effects caused by the inclination of piles are much more complex and less intuitive. The magnitude and direction of the changes experienced by the stiffness and damping functions not only depends on the presence of raked piles, the rake angle, the group configuration and the direction in which such piles are inclined, but also on the frequency range of interest. However, it can be said that, in general, for a pile group with inclined members, vertical impedances tend to decrease with the rake angle although, due to pile-soil-pile interaction effects, this tendency is not valid for all the frequency range. In this case, the varying distance between adjacent piles along its depth makes the peaks to vanish for increasing rake angles, being this a very important effect for the vertical mode. At the same time, horizontal impedances tend to increase with the rake angle when the piles are inclined in the direction of the excitation. Finally, the effect of the inclination angle on the rocking and horizontal-rocking crossed impedance functions shows a strong dependency on the specific foundation configuration. Not only the magnitude of these functions may change significantly, but the crossed impedance function may even change sign for different inclination angles, which will have an important effect on the response of the superstructure.

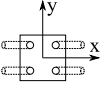
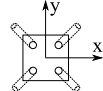
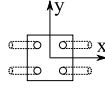
References

- [1] *Récommandations AFPS 90* Association Française de Génie Parasismique. Presses des Ponts at Chaussées: Paris, 1990.
- [2] *Eurocode 8: Design of structures for earthquake resistance. Part 5: Foundations, retaining structures and geotechnical aspects* European Committee for Standardization: Brussels, 2004.
- [3] Poulos HG. Approximate computer analysis of pile groups subjected to loads and ground movements *International Journal for Numerical and Analytical Methods in Geomechanics* 1999. **23**:1021-1041
- [4] Poulos HG. Raked piles – Virtues and drawbacks *Journal of Geotechnical and Geoenvironmental Engineering* 2006. **132**(6):795–803.
- [5] Neely WJ. Discussion of “Raked piles – Virtues and drawbacks” by Harry G. Poulos. *Journal of Geotechnical and Geoenvironmental Engineering* 2007. **133**(11):1474–1477
- [6] Deng N, Kulesza R, Ostadan F. Seismic soil-pile group interaction analysis of a battered pile group. In *Proceeding of the 4th International Conference on Earthquake Geotechnical Engineering* 2007. Thessaloniki, in CD-ROM.
- [7] Pender M. Aseismic pile foundation design. *Bulletin of the New Zealand National Society of Earthquake Engineering* 1993. **26**:49–160.
- [8] Gazetas G, Mylonakis G. Seismic soil-structure interaction: new evidence and emerging issues. In *Geotechnical Earthquake Engineering and Soil Dynamics III* ASCE, Geotechnical Special Publication II, 1998; 1119–1174.
- [9] Berrill JB, Christensen SA, Keenan RP, Okada W, Pettinga JR. Case study of lateral spreading forces on a piled foundation. *Géotechnique* 2001; **51**(6):501–517.
- [10] Guin J. *Advances in soil-pile-structure interaction and non-linear pile behavior*, Ph.D. Thesis, 1997. State University of New York at Buffalo.
- [11] Sadek M, Shahrour I. Three-dimensional finite element analysis of the seismic behavior of inclined micropiles. *Soil Dynamics and Earthquake Engineering* 2004; **24**(6):473–485.

- [12] Gerolymos N, Giannakou A, Anastasopoulos I, Gazetas G. Evidence of beneficial role of inclined piles: observations and summary of numerical analyses. *Bulletin of Earthquake Engineering* 2008; **6**(4):705–722.
- [13] Novak M, Aboul-Ella F. Impedance functions of piles in layered media. *J Eng Mech ASCE* 1978; **104**(3):643–661.
- [14] Kuhlemeyer RL. Static and dynamic laterally loaded floating piles. *J Geotech Eng ASCE* 1979; **105**:289–304.
- [15] Poulos HG, Davis EH. *Pile foundation analysis and design* John Wiley & Sons, 1980.
- [16] Kaynia AM, Kausel E. *Dynamic stiffness and seismic response of pile groups*. Report R83-03, Massachusetts Institute of Technology: Cambridge, 1982.
- [17] Dobry R, O’Rourke MJ, Roesset JM, Vicente E. Horizontal stiffness and damping of single piles. *J Geotech Eng Div, ASCE* 1982; **108**:439–459.
- [18] Sen R, Davies TG, Banerjee PK. Dynamic analysis of piles and pile groups embedded in homogeneous soils. *Earthquake Engineering & Structural Dynamics* 1985; **13**(1):53–65.
- [19] Sen R, Kausel E, Banerjee PK. Dynamic analysis of piles and pile groups embedded in non-homogeneous soils. *International Journal for Numerical and Analytical Methods in Geomechanics* 1985; **9**(6): 507–524.
- [20] Mamoon SM, Kaynia AM, Banerjee PK. Frequency domain dynamic analysis of piles and pile groups. *J Eng Mech ASCE* 1990; **116**:2237–2257.
- [21] Kaynia AM, Kausel E. Dynamics of piles and pile groups in layered soil media. *Soil Dynamics and Earthquake Engineering* 1991; **10**:386–401.
- [22] Gazetas G, Makris N. Dynamic pile-soil-pile interaction. Part I: Analysis of axial vibration. *Earthquake Engineering and Structural Dynamics* 1991; **20**:115–132.
- [23] Makris N, Gazetas G. Dynamic pile-soil-pile interaction. Part II: Lateral and seismic response. *Earthquake Engineering and Structural Dynamics* 1992; **21**:145–162.
- [24] Miura K, Kaynia AM, Masuda K, Kitamura E, Seto Y. Dynamic behaviour of pile foundations in homogeneous and non-homogeneous media. *Earthquake Engineering and Structural Dynamics* 1994; **23**:183–192.
- [25] Liu W, Novak M. Dynamic response of single piles embedded in transversely isotropic layered media. *Earthquake Engineering and Structural Dynamics* 1994; **23**:1239–1257.
- [26] Kattis SE, Polyzos D, Beskos DE. Vibration isolation by a row of piles using a 3-D frequency domain BEM. *Int J Numer Meth Eng* 1999; **46**:713–728.
- [27] Kattis SE, Polyzos D, Beskos DE. Modelling of pile wave barriers by effective trenches and their screening effectiveness. *Soil Dyn Earthquake Eng* 1999; **18**:1–10.
- [28] Maeso O, Aznárez JJ, García F. Dynamic impedances of piles and groups of piles in saturated soils. *Computers and Structures* 2005; **83**:769–782.
- [29] Sadek M, Shahrour I. Influence of the head and tip connection on the seismic performance of micropiles. *Soil Dynamics and Earthquake Engineering* 2006; **26**(6):461–468.
- [30] Giannakou A, Gerolymos , Gazetas G. On the dynamics of inclined piles. In *Proc. of the 10th International Conference on Piling and Deep Foundations* 2006. Amsterdam, The Netherlands, 286–295.

- [31] Padrón LA, Aznárez JJ, Maeso O. BEM-FEM coupling model for the dynamic analysis of piles and pile groups. *Engineering Analysis with Boundary Elements* 2007; **31**:473–484.
- [32] Padrón LA. *Numerical model for the dynamic analysis of pile foundations*, Ph.D. Thesis, 2009. University of Las Palmas de Gran Canaria. (available for download at <http://hdl.handle.net/10553/2841>)
- [33] Domínguez J. *Boundary elements in dynamics*. Computational Mechanics Publications & Elsevier Applied Science: Southampton, NY, 1993.
- [34] Vinciprova F, Maeso O, Aznárez JJ, Oliveto G. Interaction of BEM analysis and experimental testing on pile-soil systems. In *Problems in structural identification and diagnostic: General aspects and applications*. Springer-Verlag, 2003. pp. 195–227.
- [35] Gazetas G. Foundation vibrations. In *Foundation Engineering Handbook*, (2nd edn), Fang HY (ed). Kluwer/Springer Publishers, 1991; Chapter 15.

Table 1: Configurations used for validation of dynamic stiffness and damping functions

θ	10°	20°	30°
s/d	5	10	10
			

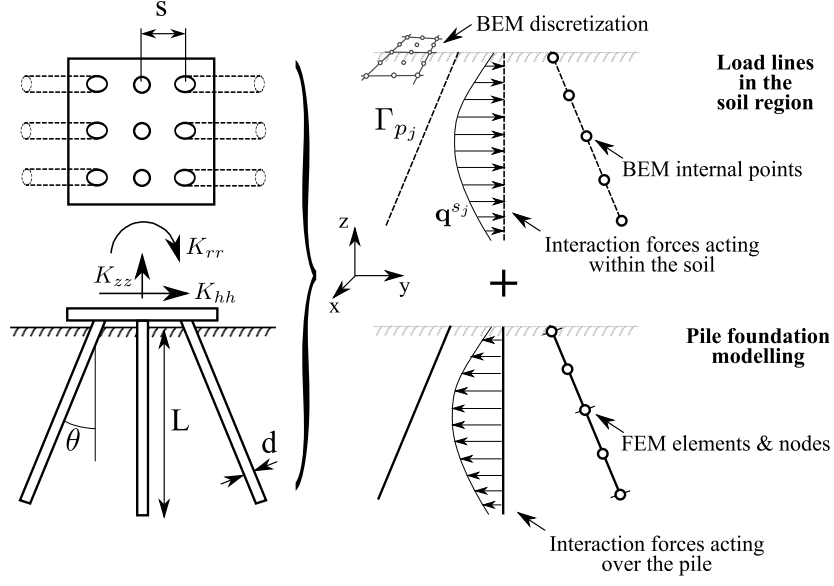


Figure 1: Pile foundation geometry and modeling through BEM-FEM coupling formulation

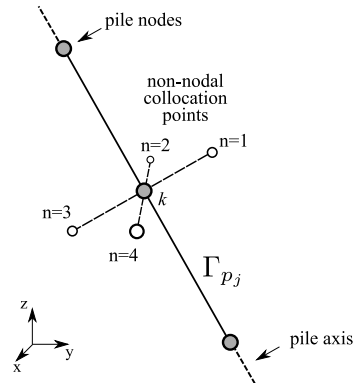


Figure 2: Placement of collocation points in non-nodal collocation strategy

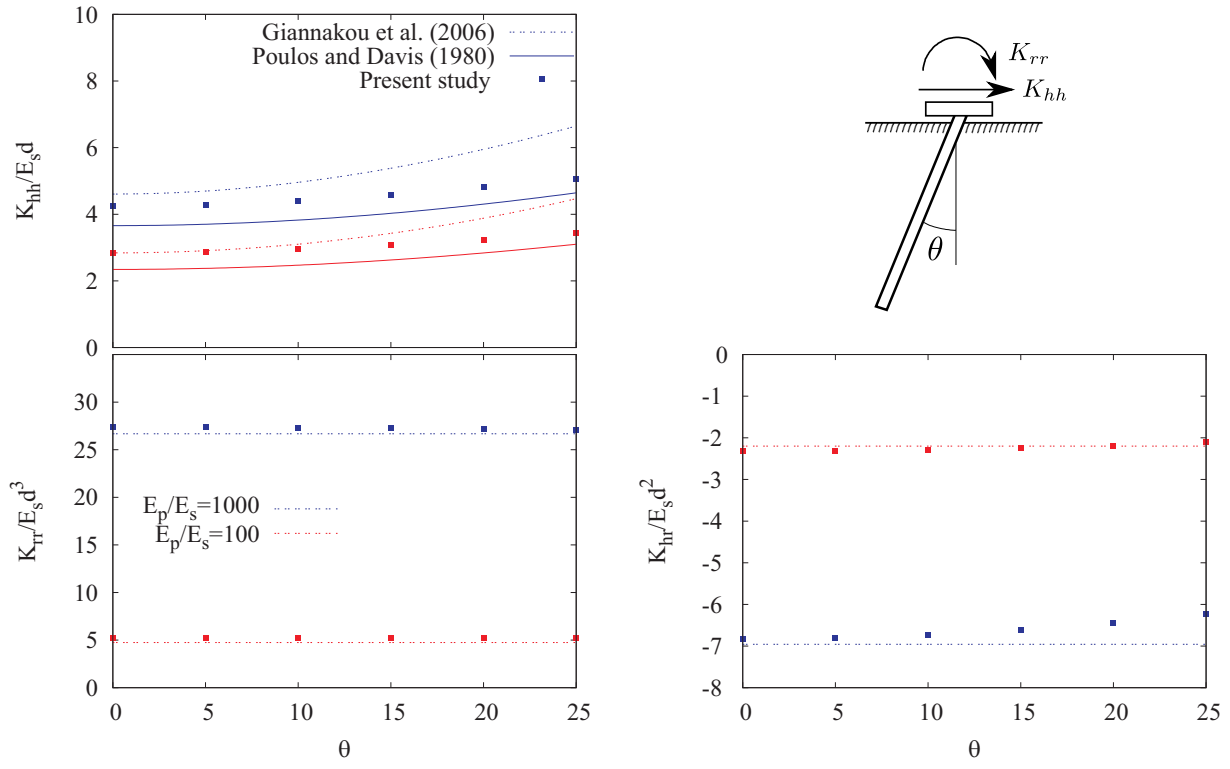


Figure 3: Static stiffness comparison results for single inclined piles.

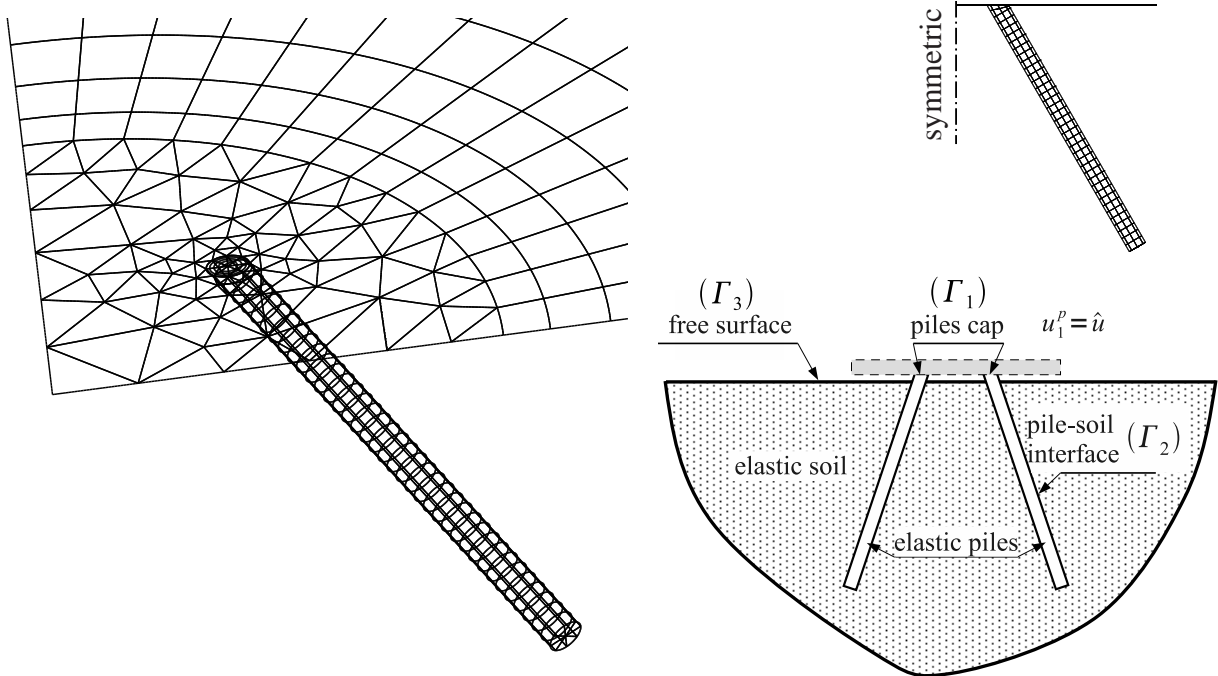


Figure 4: Multi-region boundary–element model definitions and BEM mesh details.

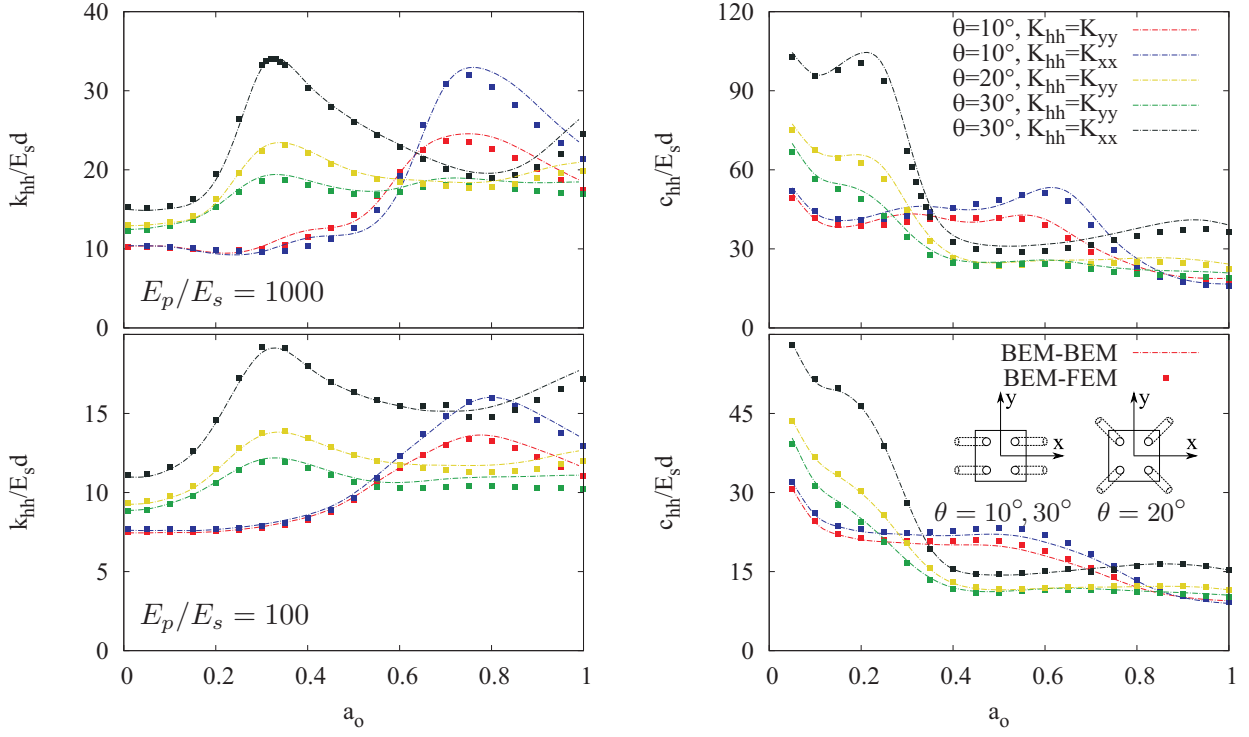


Figure 5: Comparison between horizontal impedances obtained by BEM-BEM and BEM-FEM models.

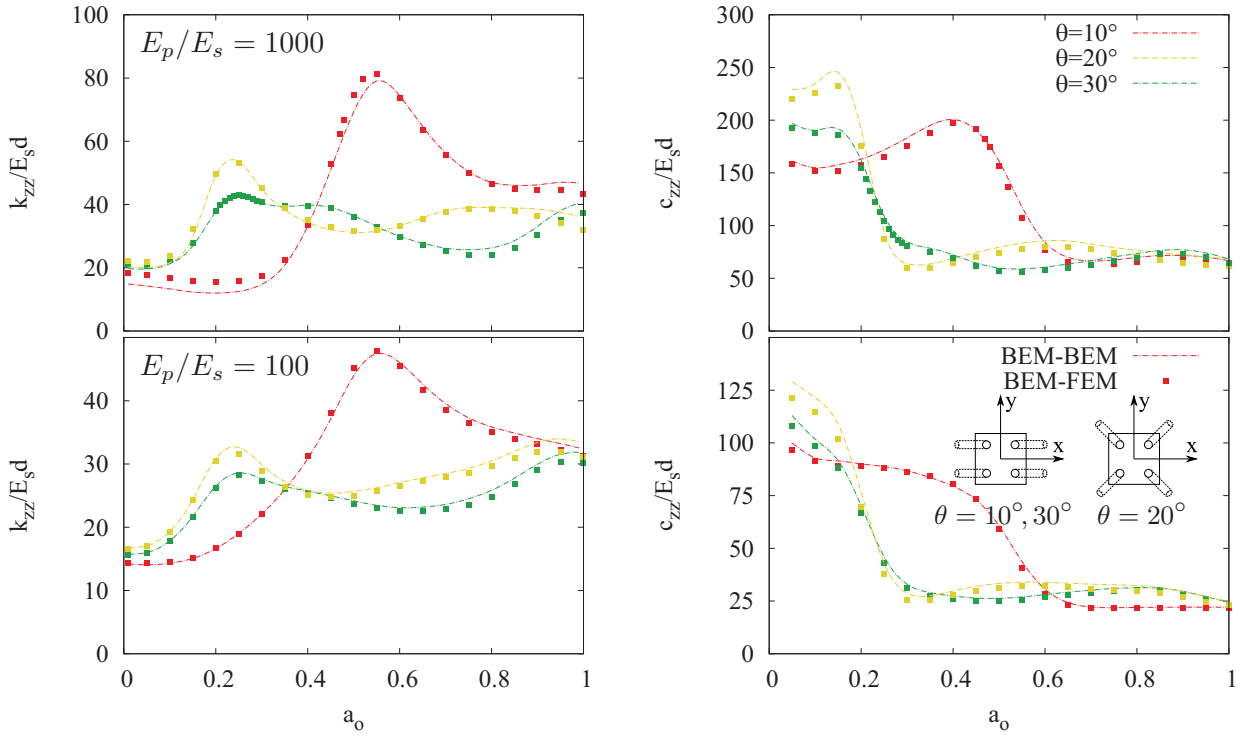


Figure 6: Comparison between vertical impedances obtained by BEM-BEM and BEM-FEM models.

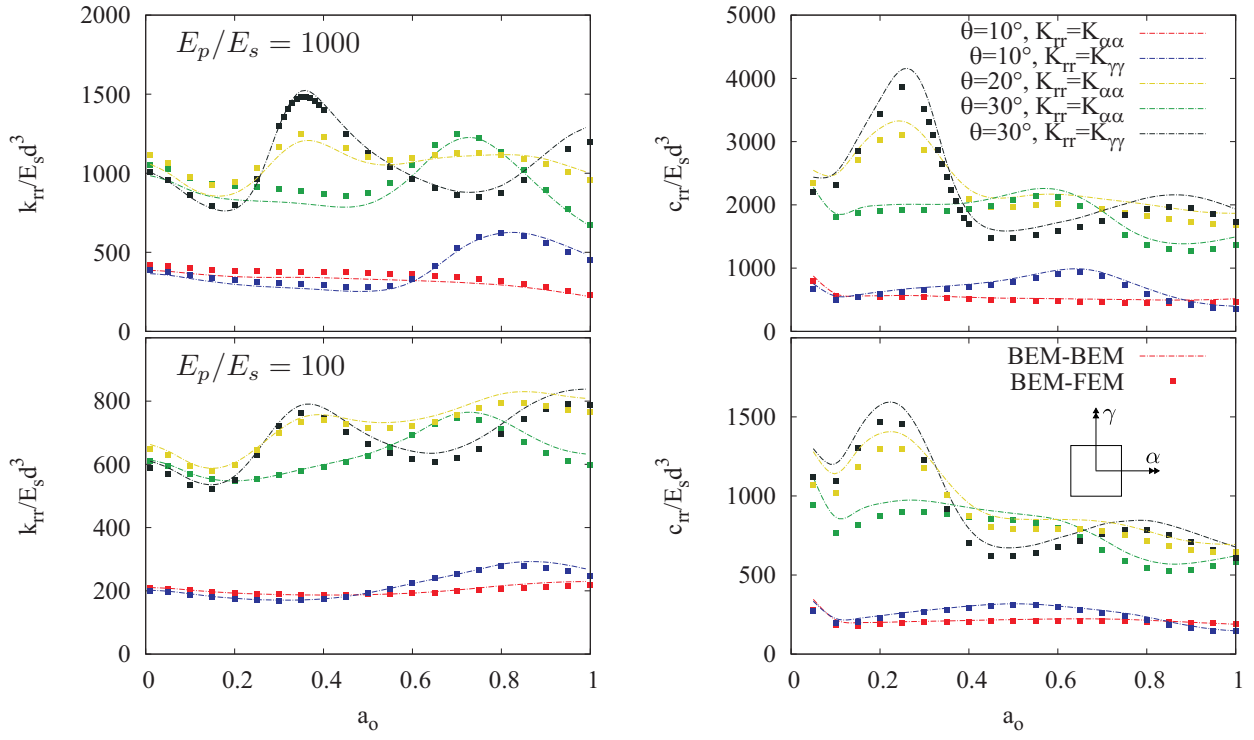


Figure 7: Comparison between rocking impedances obtained by BEM-BEM and BEM-FEM models.

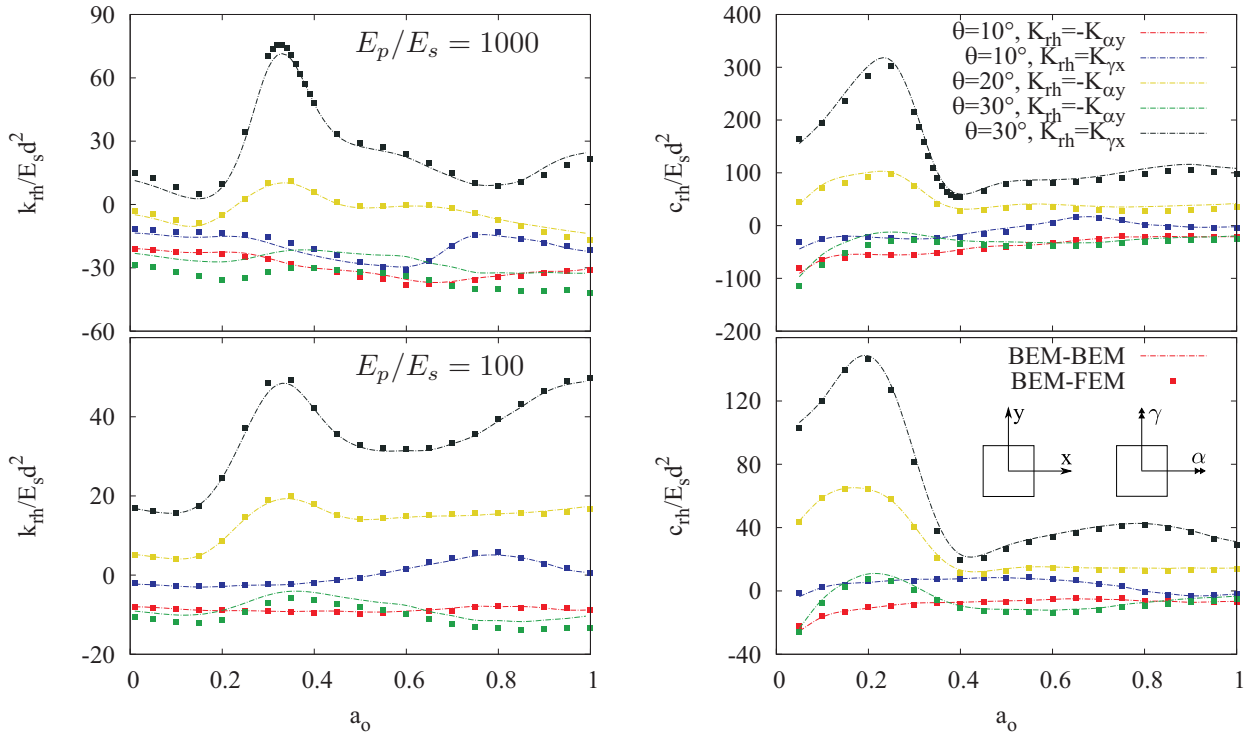


Figure 8: Comparison between horizontal-rocking crossed impedances obtained by BEM-BEM and BEM-FEM models.

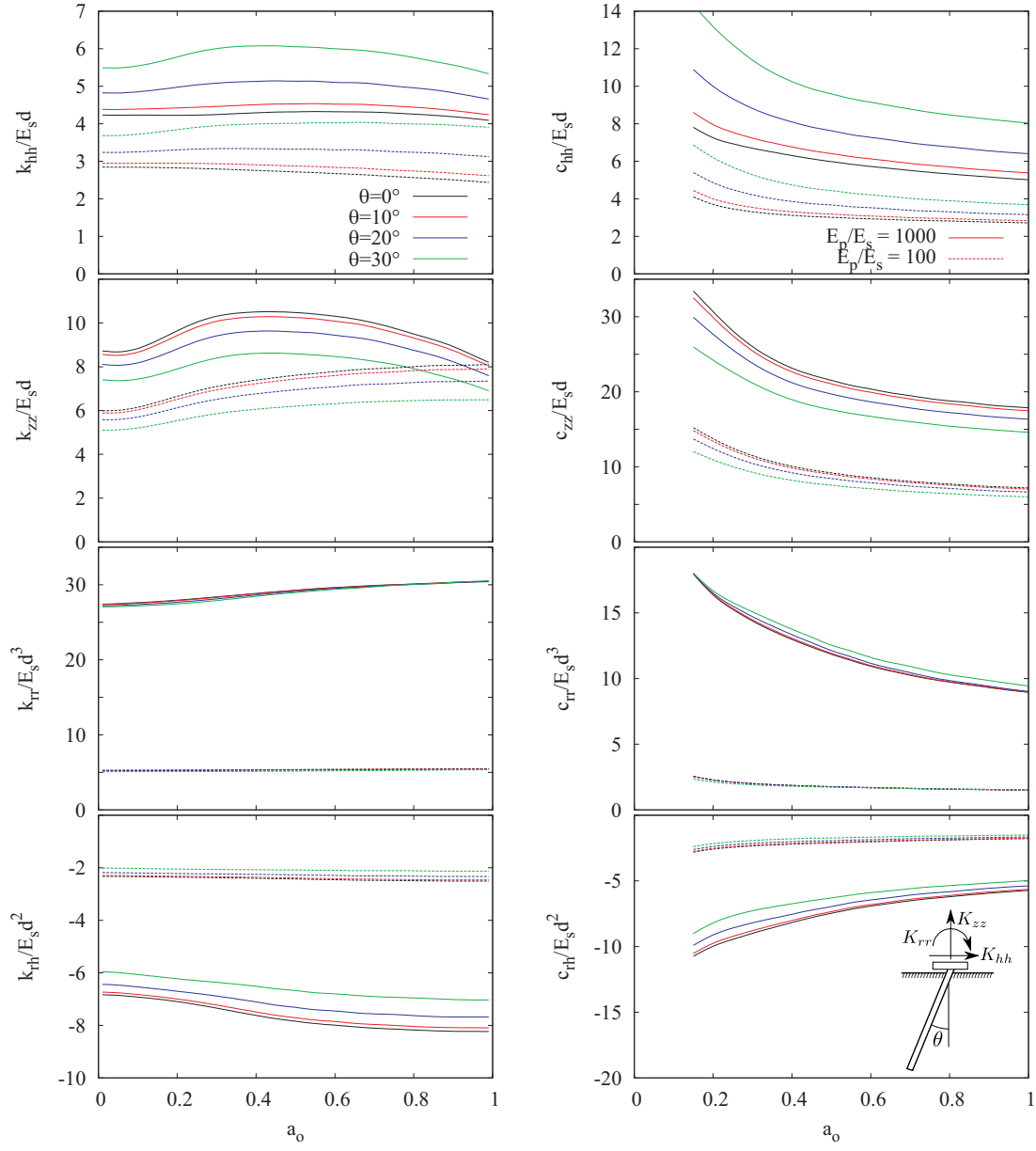


Figure 9: Impedance functions of a single inclined pile for different pile angles and stiffness ratios.

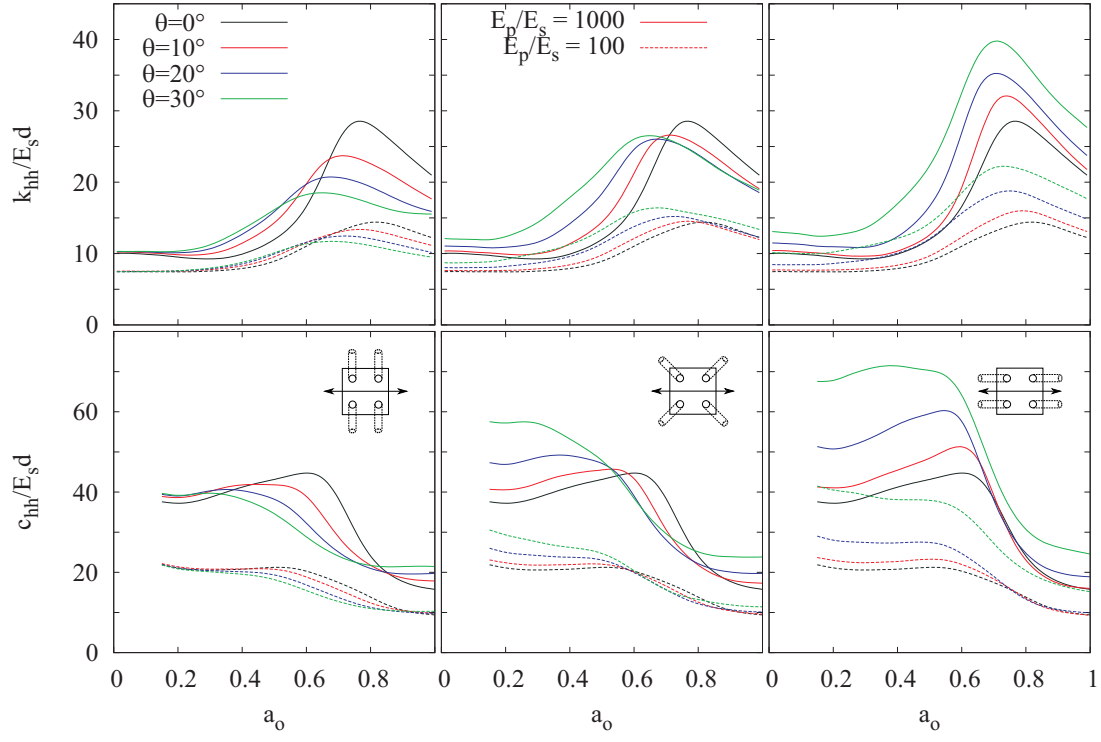


Figure 10: Horizontal impedances of 2×2 pile groups for different pile angles and stiffness ratios. $s/d=5$

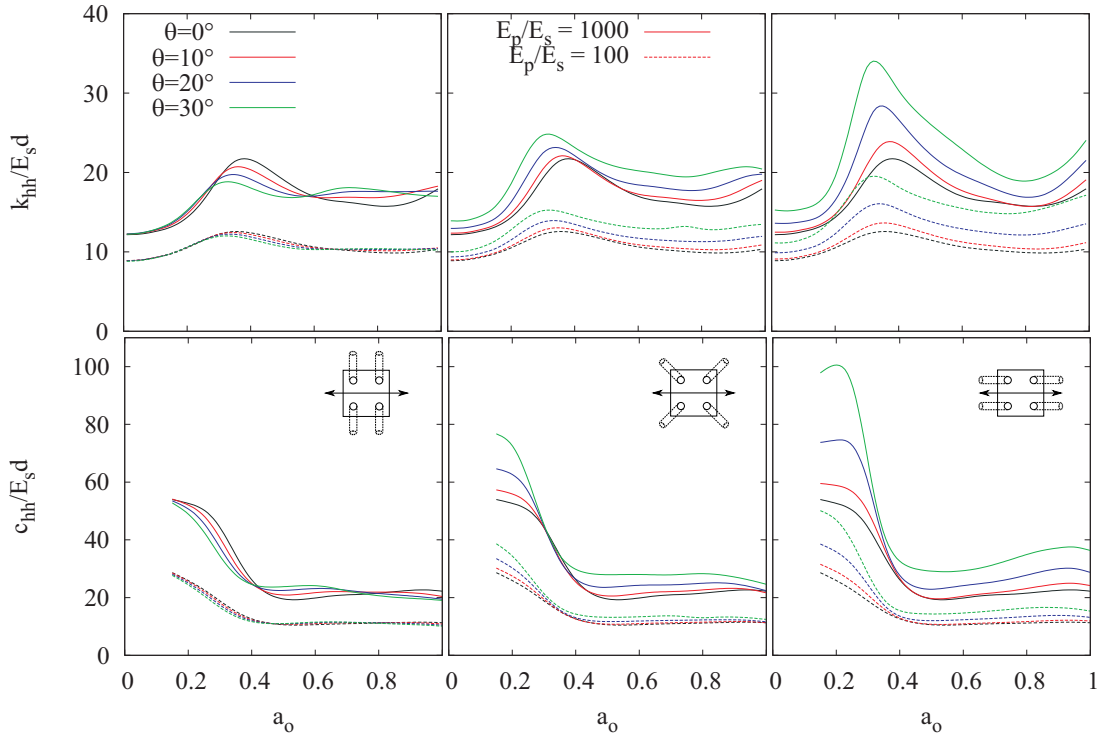


Figure 11: Horizontal impedances of 2×2 pile groups for different pile angles and stiffness ratios. $s/d=10$

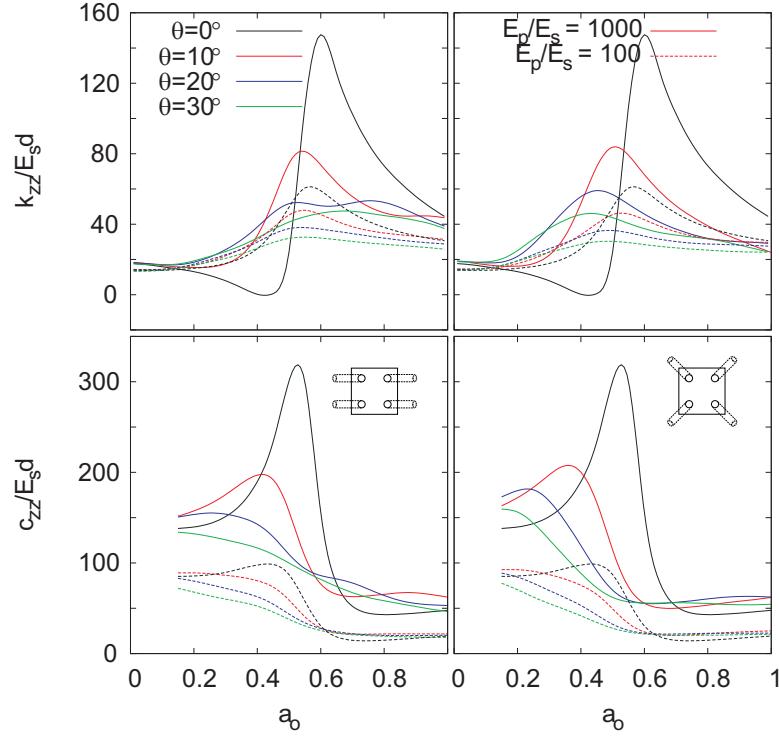


Figure 12: Vertical impedances of 2×2 pile groups for different pile angles and stiffness ratios. $s/d=5$

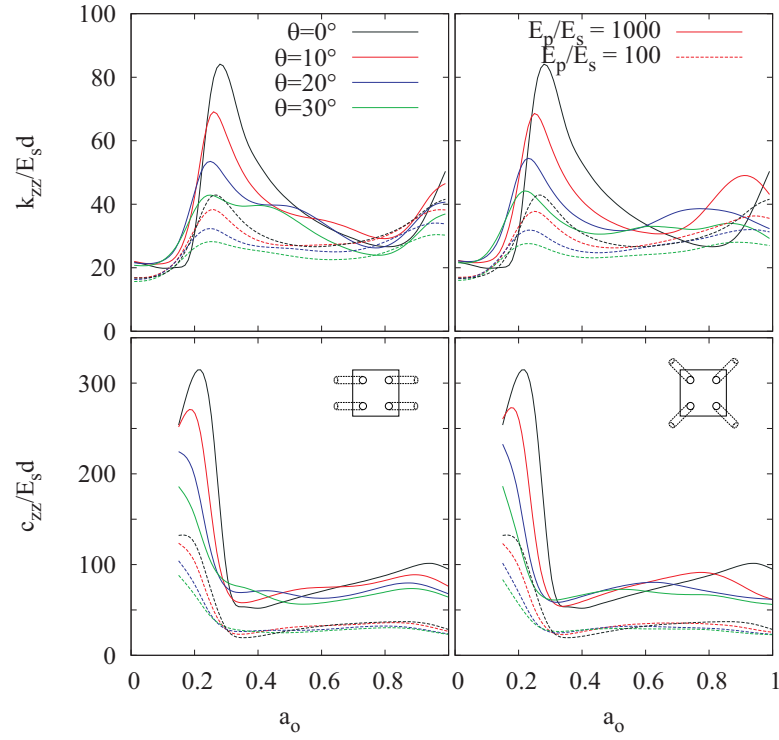


Figure 13: Vertical impedances of 2×2 pile groups for different pile angles and pile-soil stiffness ratios. $s/d=10$

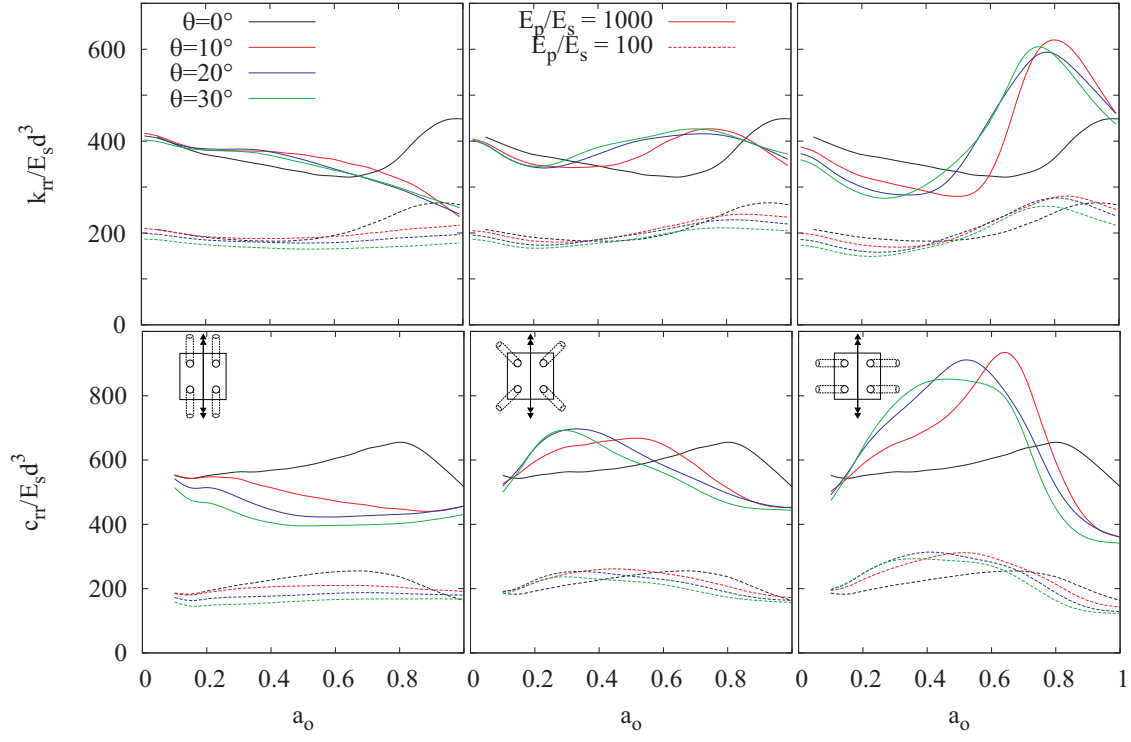


Figure 14: Rocking impedances of 2x2 pile groups for different pile angles θ and stiffness ratios. $s/d=5$

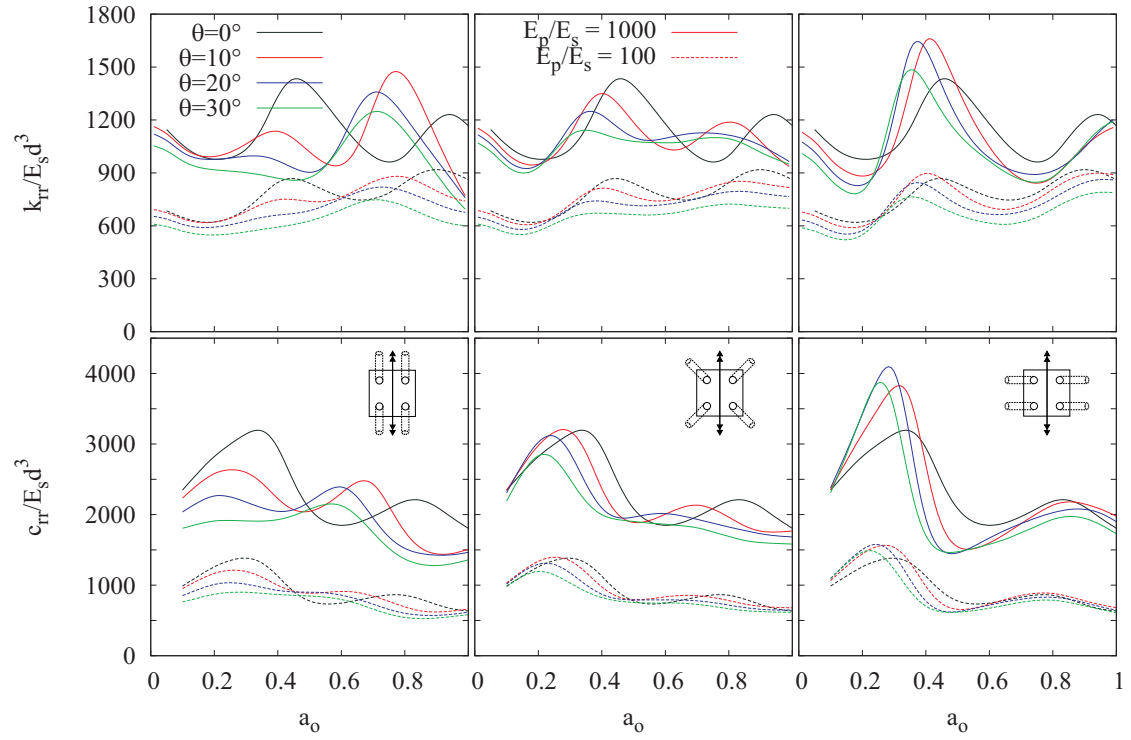


Figure 15: Rocking impedances of 2x2 pile groups for different pile angles and stiffness ratios. $s/d=10$

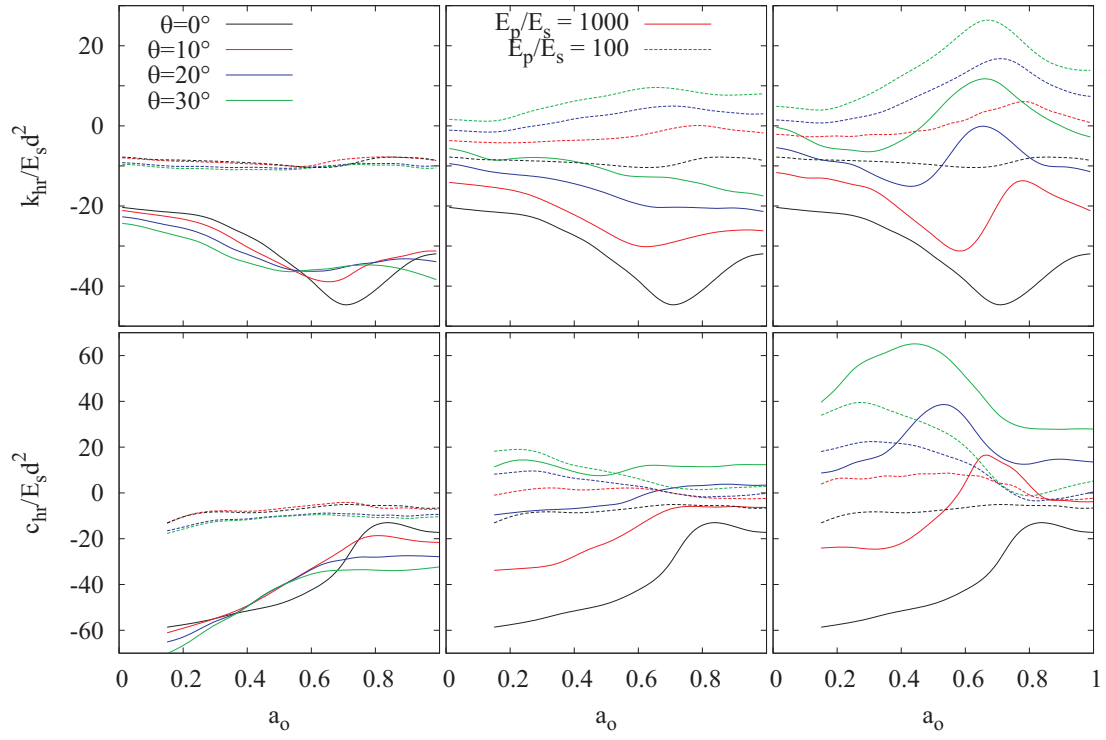


Figure 16: Horizontal-rocking crossed impedances of 2x2 pile groups for different pile angles and stiffness ratios. $s/d=5$

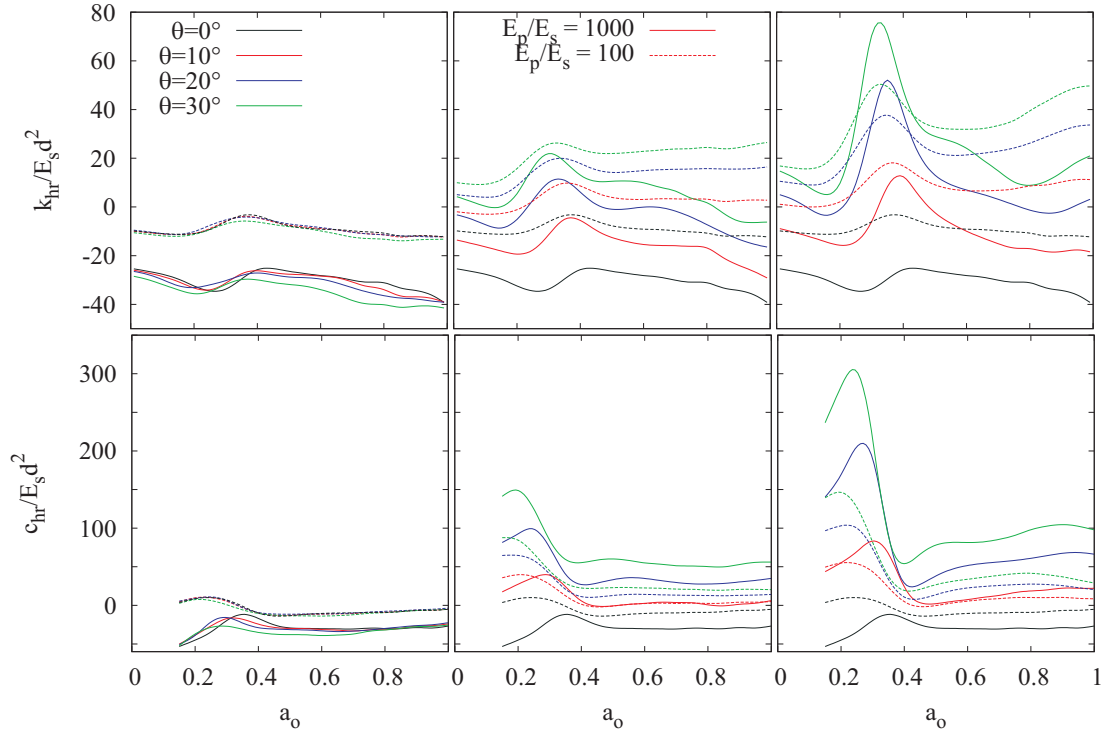


Figure 17: Horizontal-rocking cross impedances of 2×2 pile groups for different pile angles and stiffness ratios. $s/d=10$

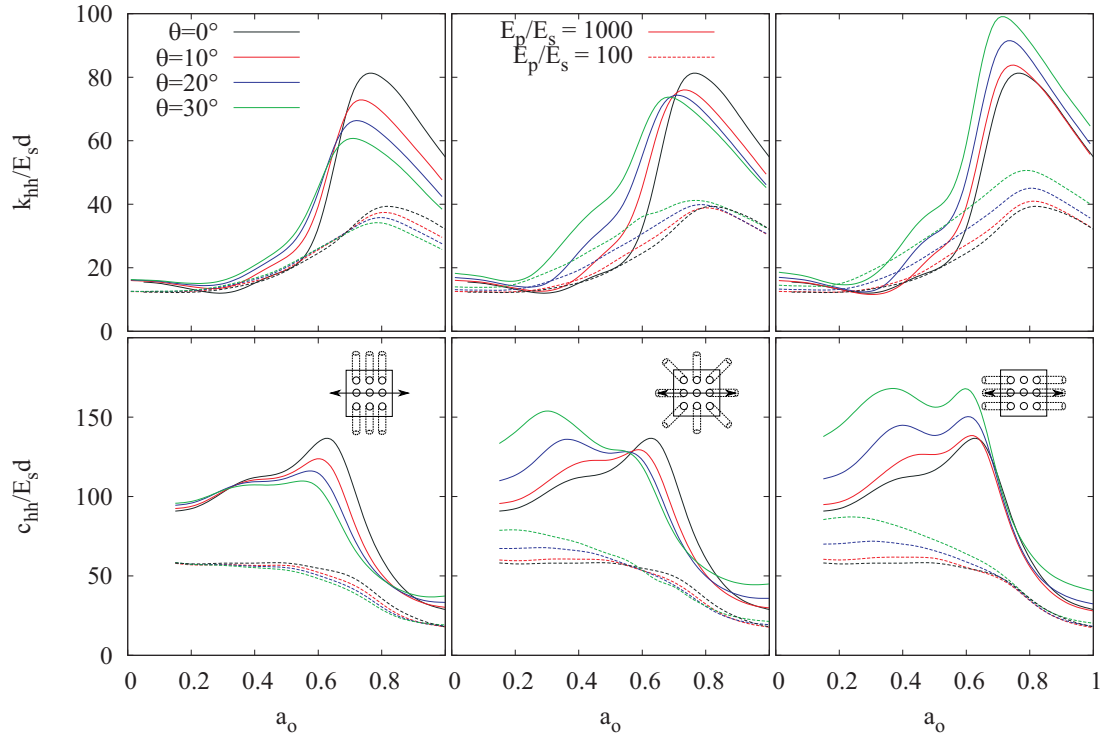


Figure 18: Horizontal impedances of 3×3 pile groups for different pile angles and stiffness ratios. $s/d=5$

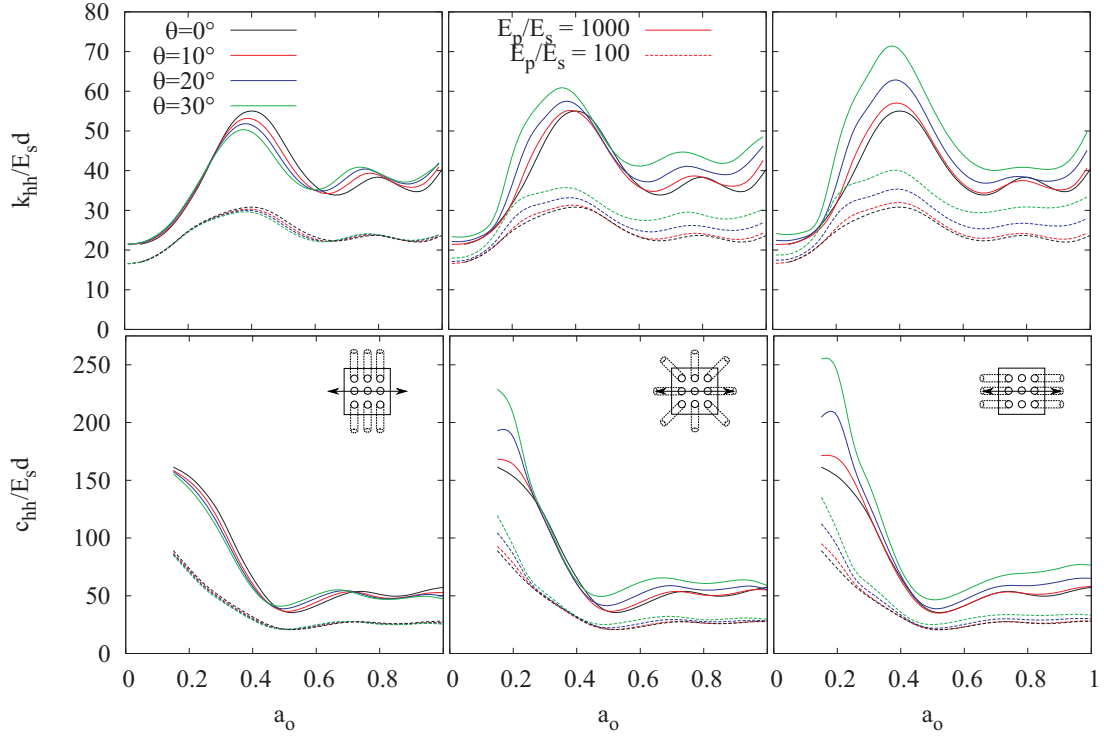


Figure 19: Horizontal impedances of 3×3 pile groups for different pile angles θ and stiffness ratios. $s/d=10$

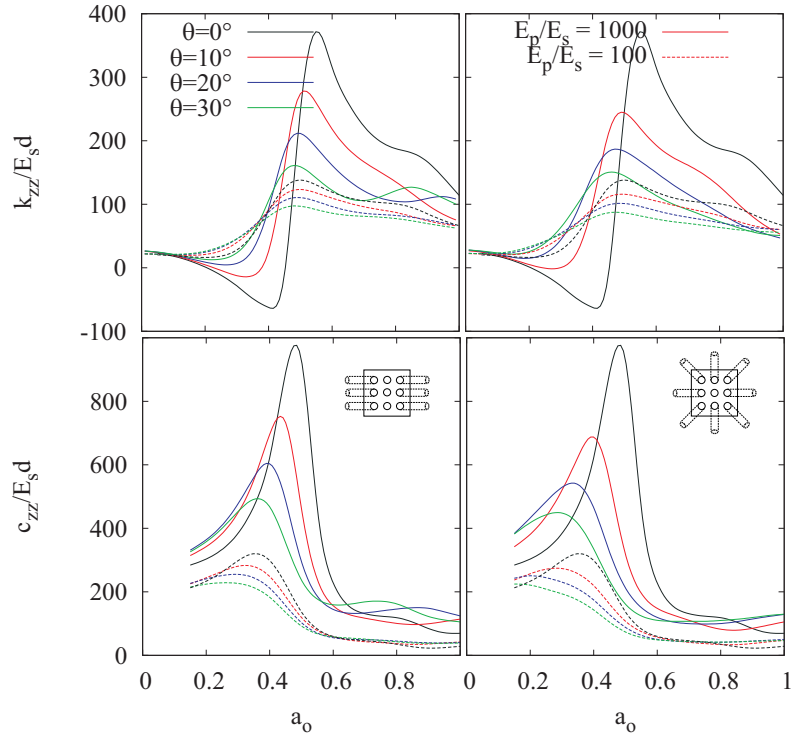


Figure 20: Vertical impedances of 3×3 pile groups for different pile angles and stiffness ratios. $s/d=5$

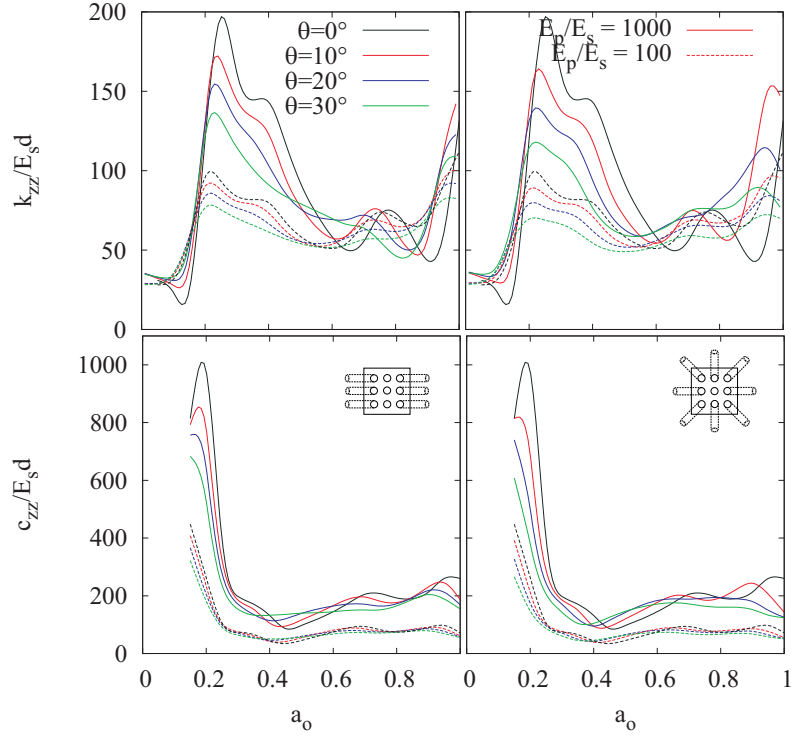


Figure 21: Vertical impedances of 3×3 pile groups for different pile angles and stiffness ratios. $s/d=10$

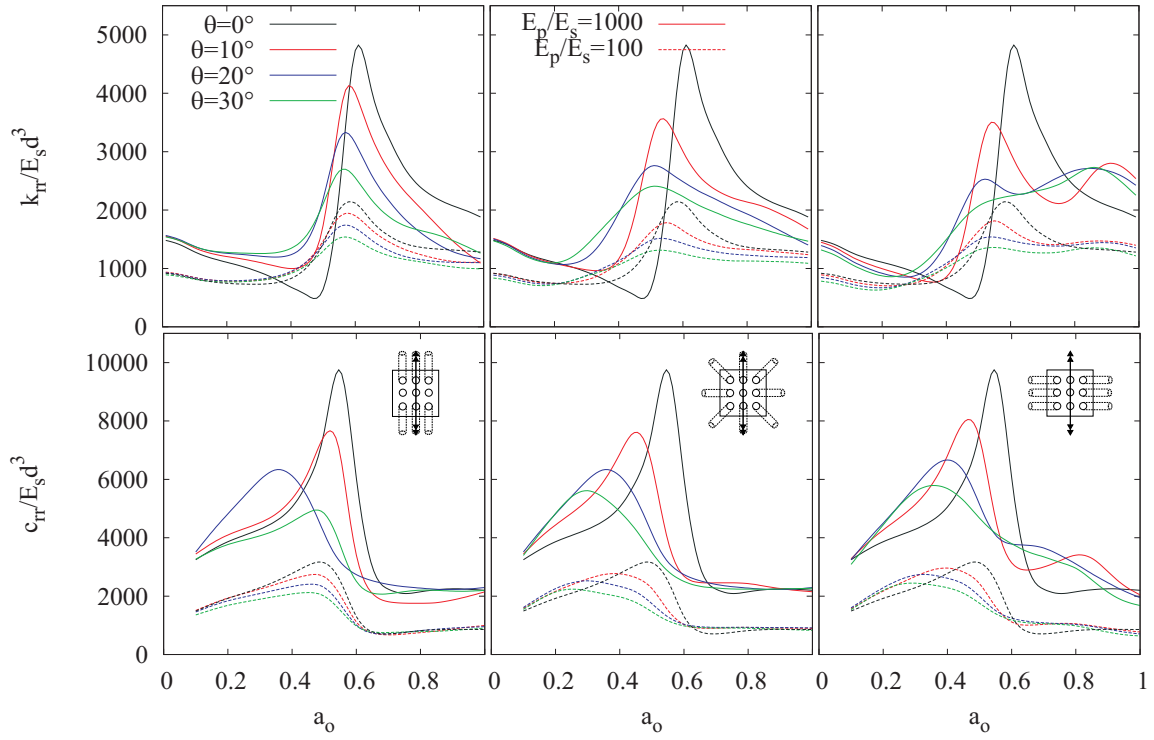


Figure 22: Rocking impedances of 3×3 pile groups for different pile angles and stiffness ratios. $s/d=5$

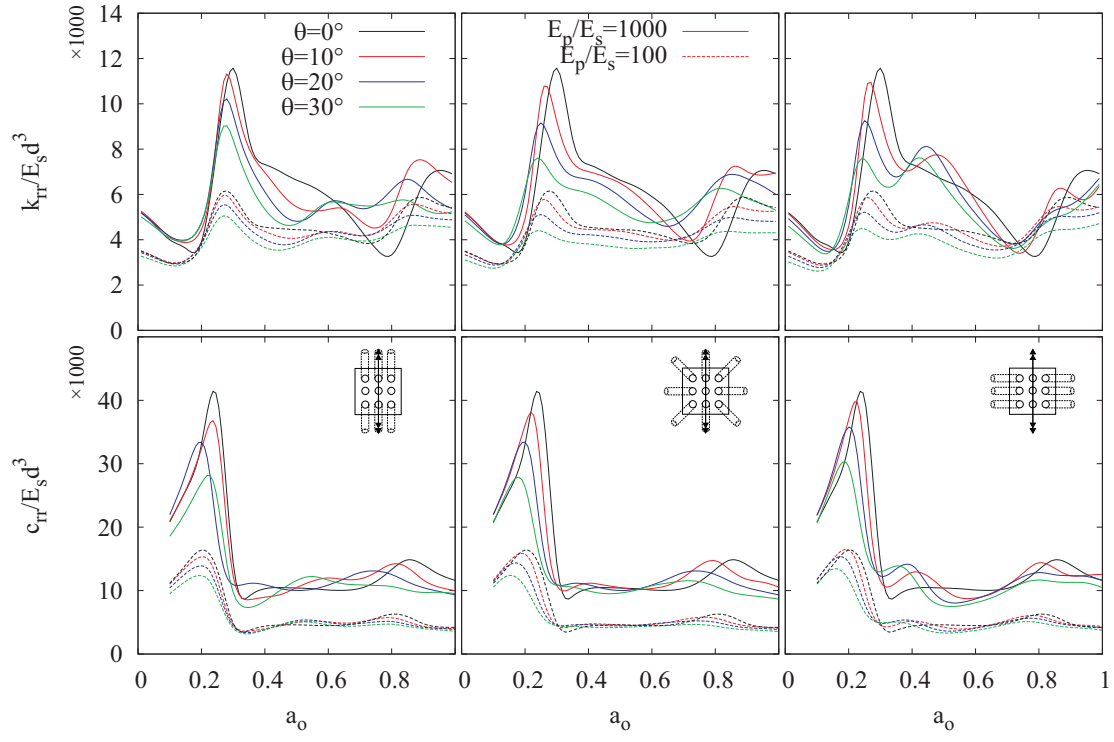


Figure 23: Rocking impedances of 3×3 pile groups for different pile angles and stiffness ratios. $s/d=10$

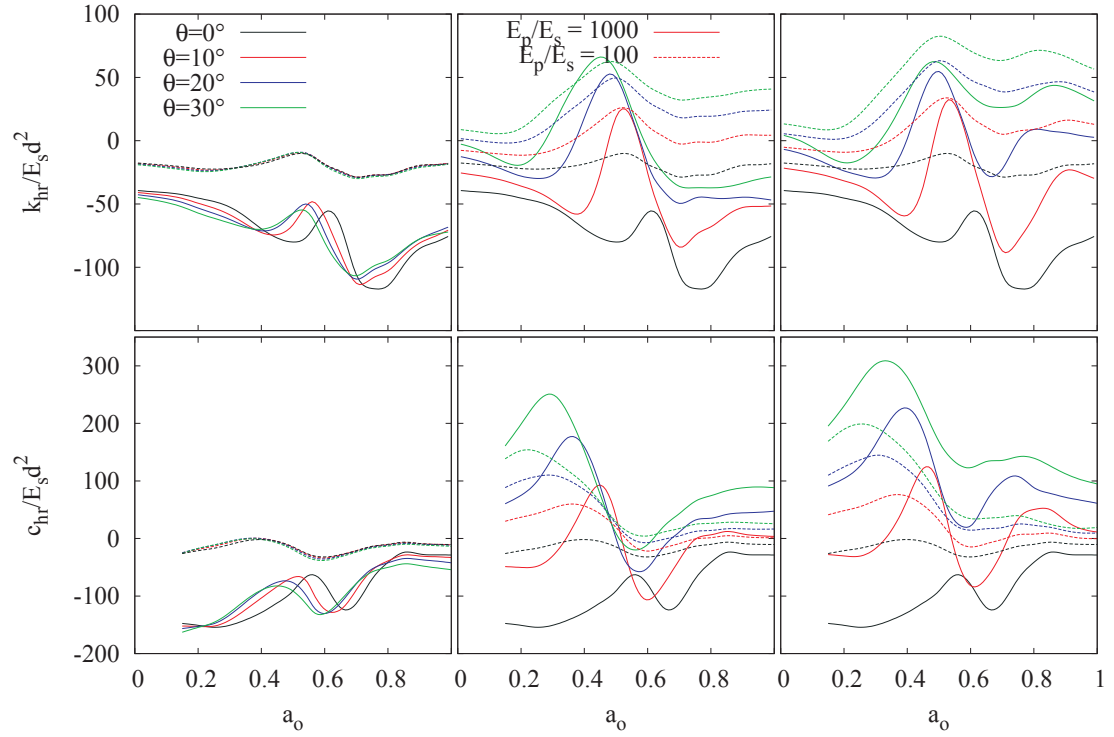


Figure 24: Horizontal-rocking crossed impedances of 3×3 pile groups for different pile angles and stiffness ratios. $s/d=5$

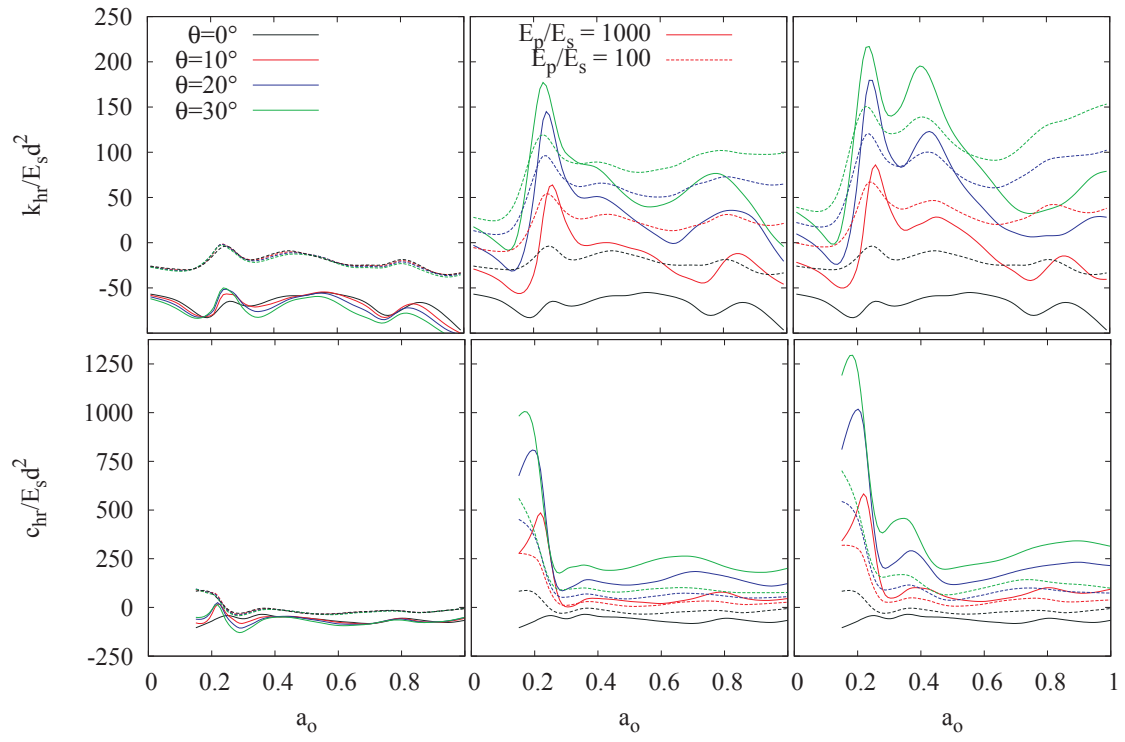


Figure 25: Horizontal-rocking crossed impedances of 3×3 pile groups for different pile angles and stiffness ratios. $s/d=10$